Supporting Information

Compression-Induced Topographic Corrugation of Air/Surfactant/Water Interface: Effect of Nanoparticles Adsorbed beneath the Interface

Inseok Chae[1], Dien Ngo[1], Mohamadamin Makarem[1], Zoubeida Ounaies[2], and Seong H. Kim[1]*

[1] Department of Chemical Engineering and Materials Research Institute, Pennsylvania State University, University Park, Pennsylvania 16802, United States

[2] Department of Mechanical Engineering and Materials Research Institute, Pennsylvania State University, University Park, Pennsylvania 16802, United States

**Corresponding author e-mail:* shkim@engr.psu.edu

A. Dimensions of cellulose nanocrystals (CNCs)

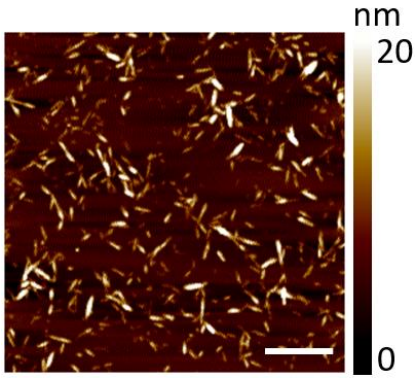

Figure S1. Extracted CNCs Iβ from Whatman No.1 filter paper. The average length and diameter of CNCs are approximately 150 nm and 8 nm, respectively. The scale bar is 1 μm.

B. Monolayer formation of DODA/CNC at the air/water interface

Coulombic interaction between cationic DODA and negatively charged CNC plays a key role in collecting CNCs from bulk water to the air/water interface.[1-2] In order to confirm this

phenomenon, Langmuir-Blodgett (LB) depositions of non-ionic surfactant (sorbitan monostearate, SorM) and no surfactant at the surface of subphase containing CNCs were also performed. 15 µl of DODA or SorM in chloroform (1 mg/ml) was spread on the surface of LB subphase (0.005 wt% CNCs in water). After the compression to 20 mN/m, 1 mm thick fused quartz substrates were vertically pulled out from the LB subphase. It was observed that surface pressure (SP) is not increased without a surfactant during the compression of barriers. The Fourier-transform infrared spectroscopy (FTIR) spectra and atomic force microscopy (AFM) images in Fig. S2 show that CNCs are deposited on the fused quartz substrate when cationic DODA molecules are spread on the subphase. On the other hand, no CNC is deposited on the fused quartz when non-ionic SorM or no surfactant is used. This confirms that the Coulombic interaction between cationic DODA head groups and negatively charged CNCs collects the CNCs from the bulk water to the air/water interface. Thickness of the deposited DODA/CNC film on the fused quartz at 60 mN/m, measured by AFM, is around 9 nm as shown in Fig. S3, which proves that the DODA/CNC at the air/water interface is a monolayer even at high SP.

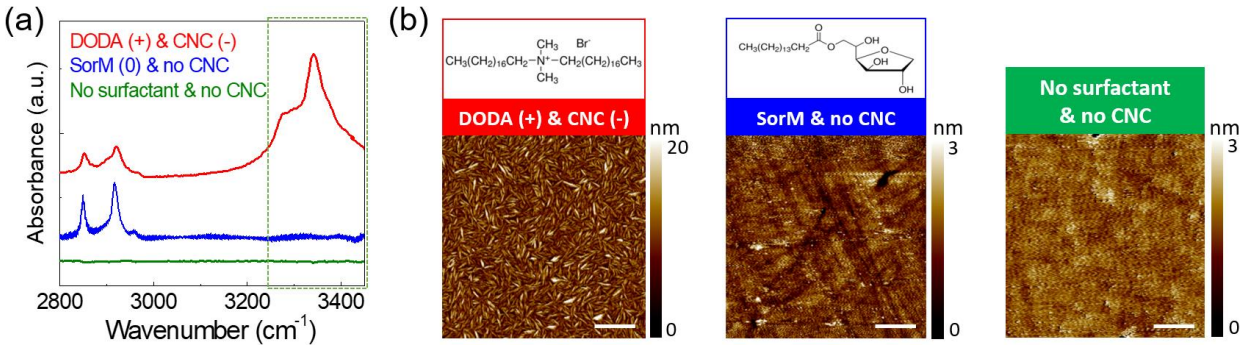

Figure S2. (a) FTIR spectra and (b) AFM images of LB films deposited on fused quartz substrates from the LB subphases containing CNCs with a cationic surfactant (red), non-ionic surfactant (blue) and no surfactant (green) at the air/water interface. (a) The IR peaks in 2800-3000 in cm^{-1} are from CH_2/CH_3 groups of DODA, SorM and CNC, and the IR peaks in 3250-3450 cm^{-1} are from OH groups of CNC. The scale bars in AFM images are 1 µm.

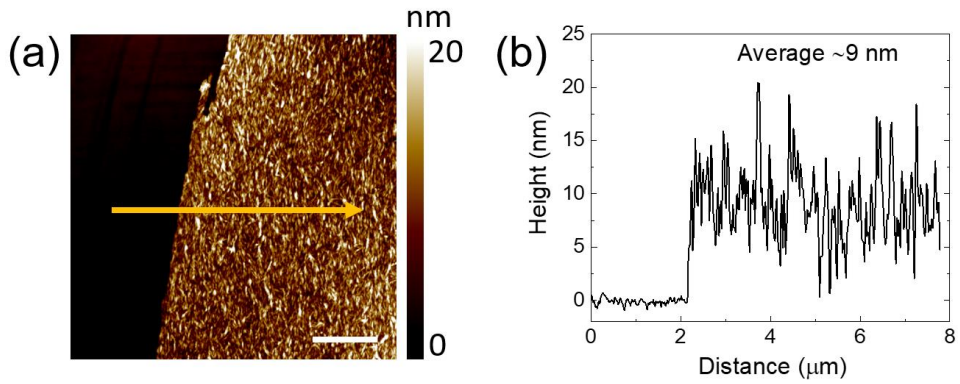

Figure S3. Thickness measurement of monolayer DODA/CNC LB film deposited on a fused quartz substrate at 60 mN/m. The height profile (b) is from the line (gold arrow) in AFM image (a). The scale bar is 2 μm.

C. Sum frequency generation (SFG) features of laterally packed CNCs

The experimental SFG features of CH/CH_2 and OH modes of CNCs (Fig 2. in manuscript) match with the time-dependent density functional theory (TD-DFT) calculation of a laterally packed CNCs in an antiparallel fashion as shown in Fig. S4. The calculation takes into account derivatives of polarizability and dipole, which decide the SFG signal, of truncated dimeric units of cellulose Iβ.[3-4] The transition dipole of OH modes have a strong directionality with respect to the chain axis of cellulose (long axis of CNC); and thus, when CNCs are arranged in the antiparallel fashion along the long axis, the OH signal is reduced due to the symmetry cancellation.[3-4] On the other hand, the transition dipole of CH/CH_2 modes have a strong directionality perpendicular to the chain axis of cellulose, which makes it more sensitive to the density.[3-5]

In the TD-DFT calculation, second order nonlinear susceptibility tensors were calculated for two cellulose crystals with an angle of 0˚, 45˚, 90˚, 135˚ and 180˚ between them using the method developed by Lee et al.[3] In order to obtain the combined second order susceptibility for the completely random case, it is assumed that cellulose crystals have an equal chance of orienting in any of the angles above, while only second order susceptibility tensor for 180˚ was considered for the antiparallel packing. In transition between completely random and antiparallel crystals, the ratio of second order susceptibility between these two packing possibilities are varied. Also, the factor of concentration is greatly important in these calculations because the crystals are randomly

arranged when the density is low, while they become laterally packed when the density is high. To incorporate the concentration factor in final SFG intensity calculation, the calculated susceptibility tensors were weighted by concentration using numbers from 0 to 100, representing low density to high density of cellulose crystals.

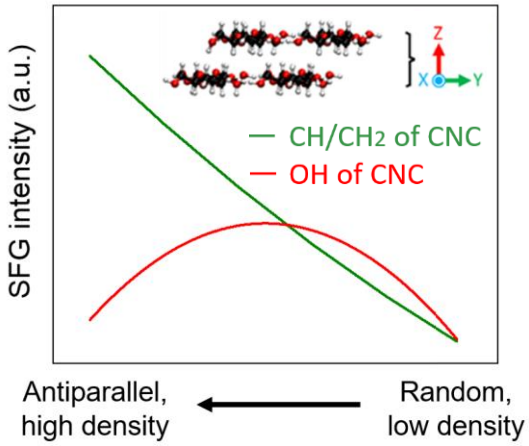

Figure S4. TD-DFT calculation of *psp*-SFG *(p*-polarized SFG, *s*-polarized VIS, *p*-polarized IR) intensity profile of CH/CH_2 and OH modes as a function of density of CNCs. The arrangements of CNCs (random at low density and antiparallel at high density) are counted in this calculation. The inset shows the crystal structure used by Lee et al.[3] to perform TD-DFT calculations. To facilitate the computational work, the cellulose crystal unit contains four truncated glucose dimers.[3]

D. DODA/CNC composites deposited on fused quartz substrates at various SPs

Fig. S5 shows the deposited DODA/CNC on fused quartz substrates at different SP. The fused quartz substrates were dipped in the LB subphase (0.005 wt% CNC in DI water) as parallel to the barriers before spreading DODA molecules on the surface of subphase. After the compression of barriers to the assigned SPs, the fused quartz substrates were vertically pulled out (1 mm/min) from the subphase. Various phases of CNCs are appeared at different SPs. At 0.5 mN/m, CNCs are not uniformly covered on the fused quartz because the density of DODA/CNC composite at the air/water surface is too low. Compressions to 1 mN/m and 10 mN/m make them more uniformly covered on the substrates, but still randomly arranged. Further compressions to 30-60 mN/m laterally pack CNCs. This result also proves that CNCs are randomly arranged at low SP but laterally packed at high SP.

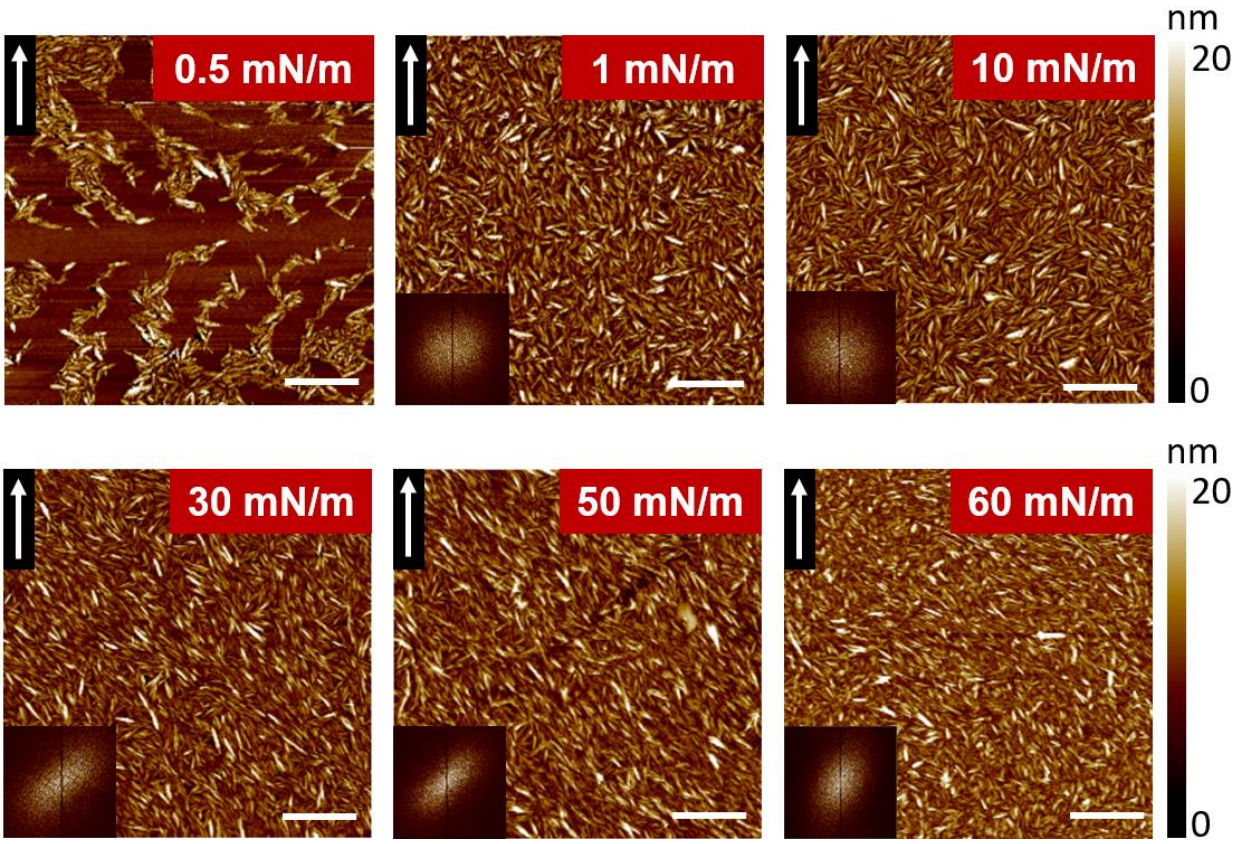

Figure S5. AFM images of DODA/CNCs on fused quartz substrates, deposited using LB trough at various SPs. Fast fourier transformation (FFT) images are included as insets. The white arrows represent a pulling direction during the LB depositions. The scale bars are 1 μm.

E. Deconvolution of d^+ and r^+ peaks of DODA in SFG spectra

In the manuscript, r^+/d^+ ratios of the SFG intensity from DODA at a single wavenumber are used in Fig. 3. To test if the intensity at single wavenumber can represent the integrated peak area, SFG peak deconvolution was performed, and then compared. The deconvolution results of r^+ and d^+ modes at various SPs are shown in Fig. S6. Linear combinations of 2848 cm^{-1} (d^+) and 2872 cm^{-1} (r^+) with Lorentzian line shapes are used. Half width at half maximum (HWHM) is fixed as 15 for 2848 cm^{-1} (d^+) and 5 for 2872 cm^{-1} (r^+). Even though the absolute values of r^+/d^+ ratios at single wavenumbers (black) are different from the integrated area ratio of deconvoluted peaks (blue), both ratios increase with the same trend. Therefore, the intensity ratios at single wavenumber can represent the actual peak ratios of r^+ and d^+ mode.

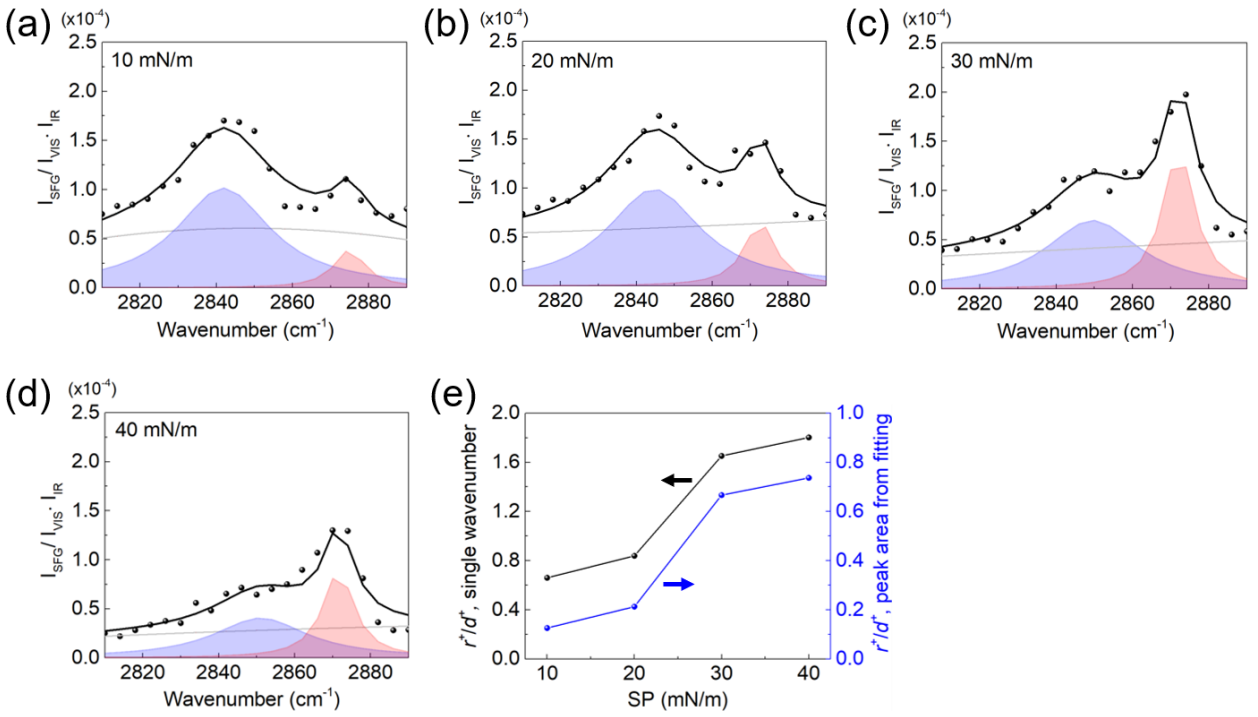

Figure S6. (a-d) Deconvolution of d^+ (2848 cm^{-1}) and r^+ (2872 cm^{-1}) modes of DODA from SFG spectrum at various SPs. (e) Comparison between the intensity ratio of r^+/d^+ at single wavenumber (black) and integrated area ratio (blue) from deconvoluted peaks.

F. SFG (*ssp*) spectrum of CNC

Fig. S7 shows the achiral *ssp*-SFG spectrum of pure CNCs. In the range of 2800-2900 cm^{-1}, relatively small peaks appear from CH_2 stretching modes. They are ~24 times smaller than the 2944 cm^{-1} peak such that they would not significantly affect the r^+/d^+ ratio of DODA in *ssp*-SFG spectrum.

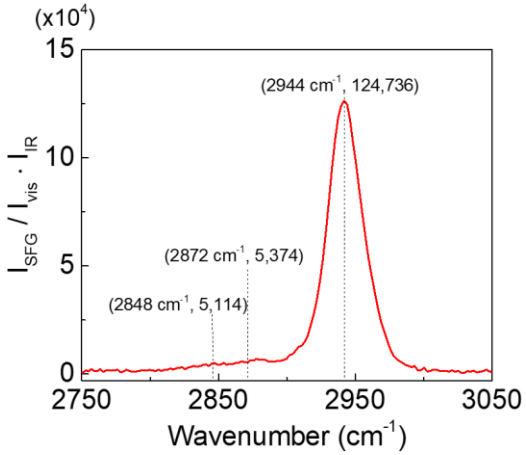

Figure S7. *ssp*-SFG spectrum of drop-cast CNCs on Si substrate.

G. Effect of surface charges on achiral SFG spectra

Electrically charged species such as DODA and CNC at the air/water interface can generate an interfacial potential Φ(0), which can affect the band shape of SFG spectra obtained with the polarization combination sensitive to achiral species (such as *ssp*).[6-8] During the LB compression, the positive surface charge density increases with DODA (+) at the water surface and the negative surface charge density increase with DODA/CNC (-) at the water surface. Generally, the achiral SFG signal (I_{SFG}) can originate from two sources when charged species exist at the interface – noncentrosymmetrically arranged functional groups and electric field effects – as shown below,[7]

$$I_{SFG} \propto |\chi^{(2)}_{total}|^2 \propto |\chi^{(2)} + \chi^{(3)}\Phi(0)|^2 \qquad (1)$$

The noncentrosymmetrically arranged molecules at the interface are responsible for the second-order susceptibility ($\chi^{(2)}$) and the electric field gradient can make the contribution from the third-order susceptibility $\chi^{(3)}\Phi(0)$ term significant.[6] The interferences among CH_2, CH_3, and OH vibrational modes and absorptive-dispersive mixing in SFG process can affect the relative intensities of resonant SFG peaks of CH_2 and CH_3 groups in the 2800-3000 cm^{-1} region.[7] In order to check whether such effects are significant or not in our experimental condition, theoretical calculations of SFG line-shapes were performed at the surface charge densities relevant to our experimental conditions following the method reported by Ohno et al.[7] The total nonlinear

susceptibility $\chi^{(2)}_{total}$ with vibrational resonances (omitting other non-resonance term) can be expressed as:[7]

$$\chi^{(2)}_{total} = \sum_{v=1}^{n} \chi^{(2)}_{res,v} e^{i\varphi_v^{(2)}} + \frac{\kappa}{\sqrt{\kappa^2 + (\Delta k_z)^2}} \chi^{(3)}_{res,v} e^{i\varphi_v^{(3)}} \Phi(0) \qquad (2)$$

where $\varphi_v^{(2)}$ and $\varphi_v^{(3)}$ are the phase angles of $\chi^{(2)}_{res,v}$ and $\chi^{(3)}_{res,v}$, respectively. κ and Δk_z are the inverse of the Debye screening length and the inverse of the coherence length of the SFG process, respectively. More details of this calculation can be found in the paper by Ohno et al.[7] The Mathematica code with modified parameters for the cases of DODA (+) and DODA/CNC (-) at the water surface is attached in the other supporting information (SI 2).

The schematics and calculated SFG spectra of the compressed DODA and DODA/CNC at the water surface are shown in Fig. S8. The optical parameters used for the highly-packed octadecyl groups of DODA were taken from the literatures reporting phase-sensitive SFG data of self-assembled monolayers of similar alkyl chains;[9] they are shown in Table S1. The phases of OH vibrational modes (up or down) at the interface after the compression should be opposite for the DODA-only (Fig. S8a) and DODA/CNC (Fig. S8b) cases. This is the reason for taking the opposite $\varphi^{(2)}$ of OH at 3200 cm^{-1} and 3400 cm^{-1} for these two cases as shown in Table S1. The phases of $\chi^{(3)}$ ($\varphi^{(3)}$) from the Debye layer (DL) were calculated using the equation[7]

$$\varphi^{(3)} = \arctan(\Delta k_z / \kappa) \qquad (3)$$

Since the ionic strength in the case of DODA-only is lower than that in the DODA/CNC case, the calculated $\varphi^{(3)}$ for DODA-only is closer to 90°.[7] The resonant peaks of CNCs are not included in the calculation because they do not have much contribution in the d^+ and r^+ region of DODA (Figure S7).

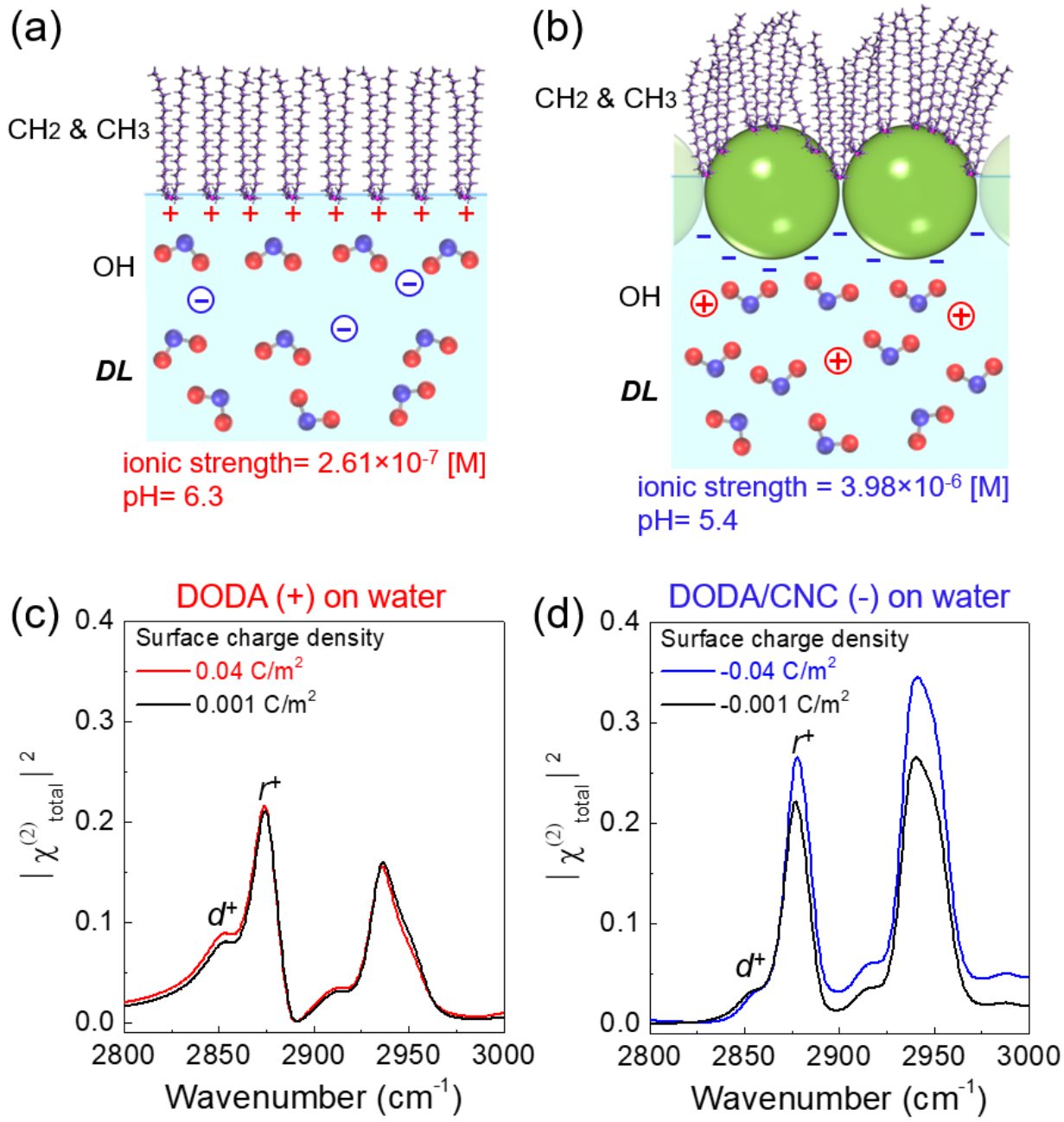

Figure S8. Schematics and calculated octadecyl-SFG spectra of (a, c) DODA (+) and (b, d) DODA/CNC (-) at the air/water interface. Optical parameters used in the calculations are shown in Table S1. The ionic strengths were calculated based on the measured pH values and sulfate groups[10] at the surface of hydrolyzed CNCs.

Table S1. Parameters of resonant peaks of CH_2 & CH_3 in DODA and OH in water used for the calculation of SFG spectra in Fig. S8c-d. The parameters of resonant peaks are from the studies reported by Wang et al.[9] and Ohno et al.[7]

(a) DODA (+) on water surface

	DODA[9]							water[7]	
Mode	Gauche defects	CH_3 (ss)	α-CH_2 (ss)	α-CH_2 (as)	CH_3 (FR)	CH_3 (as)	CH_3 (as)	OH	OH
ω_q (cm^{-1})	2854	2875	2887	2911	2934	2956	2992	$3200^{(2)}$, $3250^{(3)}$	$3400^{(2)}$, $3450^{(3)}$
$\lvert A_q^{(2)}\rvert$	1.2	4	1.4	1.4	3.1	3.2	0.2	10	10
$\varphi^{(2)}$ (°)	180	180	0	180	180	0	0	180	180
$\Gamma^{(2)}$ (cm^{-1})	10.9	8.8	7.9	13.1	8.7	10.9	9.1	120	120
$\lvert A_q^{(3)}\rvert$	·	·	·	·	·	·	·	500	150
$\varphi^{(3)}$ (°)	·	·	·	·	·	·	·	87	87
$\Gamma^{(3)}$ (cm^{-1})	·	·	·	·	·	·	·	150	150

(b) DODA/CNC (-) on water surface

	DODA[9]							water[7]	
Mode	Gauche defects	CH_3 (ss)	α-CH_2 (ss)	α-CH_2 (as)	CH_3 (FR)	CH_3 (as)	CH_3 (as)	OH	OH
ω_q (cm^{-1})	2854	2875	2887	2911	2934	2956	2992	$3200^{(2)}$, $3250^{(3)}$	$3400^{(2)}$, $3450^{(3)}$
$\lvert A_q^{(2)}\rvert$	1.2	4	1.4	1.4	3.1	3.2	0.2	10	10
$\varphi^{(2)}$ (°)	180	180	0	180	180	0	0	0	0
$\Gamma^{(2)}$ (cm^{-1})	10.9	8.8	7.9	13.1	8.7	10.9	9.1	120	120
$\lvert A_q^{(3)}\rvert$	·	·	·	·	·	·	·	500	150
$\varphi^{(3)}$ (°)	·	·	·	·	·	·	·	77	77
$\Gamma^{(3)}$ (cm^{-1})	·	·	·	·	·	·	·	150	150

As the positive surface charge density (DODA-only) increases, the resonant peak intensity of the *gauche* defects (d^+) and the CH_3 symmetric stretching modes (r^+) decreases slightly as shown in Fig. S8c. The opposite trend is observed with the negative surface charge (DODA/CNC) as shown in Fig. S8d. This is because the effective phase of $\chi^{(3)}\Phi(0)$ term is inversed by the sign change of $\Phi(0)$. The variation of resonant peaks in DODA/CNC case is larger than that of DODA at the water surface because of the higher ionic strength; as the ionic strength increases, the Debye screening length and $\frac{\kappa}{\sqrt{\kappa^2+(\Delta k_z)^2}}$ term also increase. Overall, the calculation result shows that at the

same degree of packing (Table S1), the ratio of r^+/d^+ of the octadecyl group would be higher for the DODA/CNC case (~8.0 at -0.04 C/m^2) than the DODA-only case (~2.4 at 0.04 C/m^2). The r^+/d^+ ratio increases for the DODA/CNC case as the negative surface charge density increases; however, it slightly decreases for the DODA-only case as the positive surface charge density increases. This calculation result is opposite to the experimentally-observed difference in the r^+/d^+ ratio at the compressed state (Fig. 3 in manuscript); thus, it can be surely concluded that the lower r^+/d^+ ratio for the DODA/CNC case in Fig. 3 must be associated with the lower-degree of packing of DODA molecules with the topographic corrugation formed by CNCs at the air/water interface.

References

1. Habibi, Y.; Foulon, L.; Aguié-Béghin, V.; Molinari, M.; Douillard, R., Langmuir–Blodgett Films of Cellulose Nanocrystals: Preparation and Characterization. *J. Colloid Interface Sci.* **2007,** *316* (2), 388-397.
2. Habibi, Y.; Hoeger, I.; Kelley, S. S.; Rojas, O. J., Development of Langmuir−Schaeffer Cellulose Nanocrystal Monolayers and Their Interfacial Behaviors. *Langmuir* **2010,** *26* (2), 990-1001.
3. Lee, C. M.; Chen, X.; Weiss, P. A.; Jensen, L.; Kim, S. H., Quantum Mechanical Calculations of Vibrational Sum-Frequency-Generation (SFG) Spectra of Cellulose: Dependence of the CH and OH Peak Intensity on the Polarity of Cellulose Chains within the SFG Coherence Domain. *J. Phys. Chem. Lett.* **2017,** *8* (1), 55-60.
4. Makarem, M.; Sawada, D.; O'Neill, H. M.; Lee, C. M.; Kafle, K.; Park, Y. B.; Mittal, A.; Kim, S. H., Dependence of Sum Frequency Generation (SFG) Spectral Features on the Mesoscale Arrangement of SFG-Active Crystalline Domains Interspersed in SFG-Inactive Matrix: A Case Study with Cellulose in Uniaxially Aligned Control Samples and Alkali-Treated Secondary Cell Walls of Plants. *J. Phys. Chem. C* **2017,** *121* (18), 10249-10257.
5. Lee, C. M.; Kafle, K.; Park, Y. B.; Kim, S. H., Probing Crystal Structure and Mesoscale Assembly of Cellulose Microfibrils in Plant Cell Walls, Tunicate Tests, and Bacterial Films Using Vibrational Sum Frequency Generation (SFG) Spectroscopy. *Phys. Chem. Chem. Phys.* **2014,** *16* (22), 10844-10853.
6. Wen, Y.-C.; Zha, S.; Liu, X.; Yang, S.; Guo, P.; Shi, G.; Fang, H.; Shen, Y. R.; Tian, C., Unveiling Microscopic Structures of Charged Water Interfaces by Surface-Specific Vibrational Spectroscopy. *Phys. Rev. Lett.* **2016,** *116* (1), 016101.
7. Ohno, P. E.; Wang, H.-f.; Geiger, F. M., Second-Order Spectral Lineshapes from Charged Interfaces. *Nat. Commun.* **2017,** *8* (1), 1032.
8. Urashima, S.-h.; Myalitsin, A.; Nihonyanagi, S.; Tahara, T., The Topmost Water Structure at a Charged Silica/Aqueous Interface Revealed by Heterodyne-Detected Vibrational Sum Frequency Generation Spectroscopy. *J. Phys. Chem. Lett.* **2018,** *9* (14), 4109-4114.
9. Wang, J.; Bisson, P. J.; Marmolejos, J. M.; Shultz, M. J., Nonlinear Interferometer: Design, Implementation, and Phase-Sensitive Sum Frequency Measurement. *J. Chem. Phys.* **2017,** *147* (6), 064201.
10. Roman, M.; Winter, W. T., Effect of Sulfate Groups from Sulfuric Acid Hydrolysis on the Thermal Degradation Behavior of Bacterial Cellulose. *Biomacromolecules* **2004,** *5* (5), 1671-1677.